bioRxiv preprint doi: https://doi.org/10.1101/2021.02.28.433294; this version posted March 1, 2021. The copyright holder for this preprint (which was not certified by peer review) is the author/funder. All rights reserved. No reuse allowed without permission.

Selective attention and decision-making have separable neural bases in space and time

Authors: Denise Moerel[1,2], Anina N. Rich[1,2,3,*], & Alexandra Woolgar[1,2,4,*]

[*] Equal contribution

1. Department of Cognitive Science, Macquarie University, Sydney, Australia
2. Perception in Action Research Centre, Macquarie University, Sydney, Australia
3. Centre for Elite Performance, Expertise and Training, Macquarie University, Sydney, Australia
4. MRC Cognition and Brain Sciences Unit, University of Cambridge, Cambridge, United Kingdom

ABSTRACT

Attention and decision-making processes are fundamental to cognition. However, they are usually experimentally confounded, making it impossible to link neural observations to specific processes. Here we separated the effects of selective attention from the effects of decision-making in human observers using a two-stage task where the attended stimulus and decision were orthogonal and separated in time. Multivariate pattern analyses of multimodal neuroimaging data revealed the dynamics of perceptual and decision-related information coding through time (magnetoencephalography (MEG)), space (functional Magnetic Resonance Imaging (fMRI)), and their combination (MEG-fMRI fusion). Our MEG results showed an effect of attention before decision-making could begin, and fMRI results showed an attention effect in early visual and frontoparietal regions. Model-based MEG-fMRI fusion suggested that attention boosted stimulus information in frontoparietal and early visual regions before decision-making was possible. Together, our results suggest that attention affects neural stimulus representations in frontoparietal regions independent of decision-making.

bioRxiv preprint doi: https://doi.org/10.1101/2021.02.28.433294; this version posted March 1, 2021. The copyright holder for this preprint (which was not certified by peer review) is the author/funder. All rights reserved. No reuse allowed without permission.

1. INTRODUCTION

Selective attention is a mechanism that prioritises relevant information from amongst competing sensory input. With clear behavioural benefits to attending to particular locations in space (Pestilli & Carrasco, 2005; Posner, 1980) or to particular visual features (Sàenz et al., 2003; White & Carrasco, 2011), there is strong evidence that attention affects perception (Carrasco, 2011). However, in cognitive neuroscience experiments, the selection and maintenance of relevant stimulus information is commonly confounded with decision-making processes that pertain to the selected input. We address this ambiguity by separating the effects of attentional selection and maintenance on the neural processing of information from the effects of decision-making to study of the spatiotemporal correlates of each process separately.

The adaptive coding hypothesis (Duncan, 2001) proposes a framework for how selective attention could affect stimulus processing. According to this hypothesis, single cells in frontoparietal cortex can flexibly adapt their response to code different information as needed for the task, which provides a potential source of bias for more selective brain regions (Desimone & Duncan, 1995). Accordingly, single cell recordings in non-human primates show task-dependent neural tuning profiles in prefrontal cortex (Rao et al., 1997; Sigala et al., 2008; Stokes et al., 2013), with an emphasis on coding information that is currently relevant for the task (Kadohisa et al., 2013). In humans, a network of frontoparietal regions also responds with a profile consistent with adaptive coding. We will use the term 'Multiple Demand' (MD) regions (Duncan, 2010; Duncan & Owen, 2000) to refer to this frontoparietal network, but similar networks have been referred to as the 'frontoparietal control system' (Vincent et al., 2008), 'task positive network' (Fox et al., 2005), and 'task activation ensemble' (Seeley et al., 2007). Functional Magnetic Resonance Imaging (fMRI) studies in human participants show that the MD regions respond to a wide range of

bioRxiv preprint doi: https://doi.org/10.1101/2021.02.28.433294; this version posted March 1, 2021. The copyright holder for this preprint (which was not certified by peer review) is the author/funder. All rights reserved. No reuse allowed without permission.

cognitively demanding tasks (Assem et al., 2020; Dosenbach et al., 2006; Duncan & Owen, 2000; Fedorenko et al., 2013).

More specific evidence for an adaptive response in the MD regions comes from studies that use multivariate pattern analyses (MVPA) to test for the contents of the neural representations, using the patterns of response across voxels (fMRI) or sensors (MEG) (see Grootswagers et al., 2016; Haynes, 2015; Hebart & Baker, 2017). Studies using this technique on fMRI data show that multivariate patterns of activity code for a range of task-relevant information in different contexts (Woolgar et al., 2016), with single MD voxels re-used to code multiple task features between tasks (Jackson & Woolgar, 2018). In addition, Woolgar and colleagues (2015) found stronger visual object coding in the MD cortex for cued (i.e., attended, task-relevant) objects relative to equivalent distractor objects, and Jackson and colleagues (2016) reported stronger MD coding of cued compared to equivalent distractor features of the same object. Moreover, MD coding of cued information can be selectively impaired by non-invasive stimulation the right dorsolateral prefrontal cortex, one of the nodes in the MD network (Jackson et al., 2020). In parallel, recent magnetoencephalography (MEG) studies have shown the coding of a cued feature at a cued location is sustained over time, while information coding for distractor information is not sustained (Battistoni et al., 2018; Goddard et al., 2019). What we do not know, however, is whether this difference in information coding between cued and distractor stimuli is driven by the attentional selection and maintenance of relevant information or, at least partially, by decision-making processes pertaining to that information. In most paradigms, including those used in the studies outlined above, attention is manipulated by asking participants to respond to the cued (but not the distractor) stimulus. As decisions pertain to the cued information only, attending to a stimulus and making a decision about the stimulus could both contribute to previous findings.

bioRxiv preprint doi: https://doi.org/10.1101/2021.02.28.433294; this version posted March 1, 2021. The copyright holder for this preprint (which was not certified by peer review) is the author/funder. All rights reserved. No reuse allowed without permission.

Underscoring the importance of this confound, there is clear evidence that decisions can drive decoding, although these studies do not explicitly investigate the role of attention. For instance, decisions can be decoded from early visual areas (Löffler et al., 2019; Rens et al., 2017), as well as from frontoparietal cortex (Löffler et al., 2019). In these paradigms, the decision was not driven by visual information, as participants had to make a choice between multiple options. Bode and colleagues (2012) found perceptual decisions could be decoded from 140-180ms post-stimulus onwards from pure noise images. This is a similar time-course as the effect of attention on stimulus coding (Goddard et al., 2019). Thus, decisions can be decoded in similar areas of the brain, and with a similar time-course as effects of attention, further complicating interpretation of the extant literature.

There is, however, some evidence suggesting that effects of attention can occur in the absence of decision-making processes. For example, in a univariate fMRI study, Hon and colleagues (2006) showed activation in the MD regions in response to changes in cued streams, but not in distractor streams of stimuli. This occurred even when the participant did not have to respond or did an orthogonal task. This study links attention to overall changes in blood flow to MD regions but did not investigate what information was coded about the attended and unattended stimuli.

Here, we used MVPA of MEG and fMRI data to address 3 research questions. First, we asked whether attention affects the coding of stimulus information when it is separated from decision-making processes in time. We used the high temporal resolution of MEG in combination with a 2-stage task to dissociate the coding of attended and unattended visual information from coding of decision-related information. Our data showed that relevant information was prioritised during the first stage, showing a clear effect of selecting and maintaining specific features before participants could make a decision. Second, we used fMRI to ask what type of information the MD regions hold. The results showed that the MD regions preferentially code visual information when it is cued as relevant, compared to when

bioRxiv preprint doi: https://doi.org/10.1101/2021.02.28.433294; this version posted March 1, 2021. The copyright holder for this preprint (which was not certified by peer review) is the author/funder. All rights reserved. No reuse allowed without permission.

the same visual information is a distractor, *as well as* the orthogonal decisions about the stimuli needed to generate a response. This suggests the MD regions are involved both in supporting selective attention and in decision-making. Finally, we used model-based MEG-fMRI to formally combine the data from the two imaging modalities and examine the time-course with which the MD regions preferentially coded for cued compared to distractor information during the first phase of the trial. The results suggest that the MD regions selectively code for cued visual information *before* decision-making begins in this task. These data show that while similar brain regions are involved in both attention and decision-making, the two processes are separable with distinct spatiotemporal neural correlates.

2. MATERIALS AND METHODS

2.1. MEG acquisition and analysis

2.1.1. Participants

The first part of this study consisted of a behavioural training session and a MEG session carried out at Macquarie University (Sydney, Australia). We tested 31 healthy volunteers in the behavioural training session. Of these, 21 performed well enough to participate in the MEG session (at least 90% accuracy in the final run of the training session). The MEG data from 1 participant were excluded due to a failure to complete the experiment, resulting in a final MEG sample of 20 participants (14 female/6 male, 18 righthanded/2 lefthanded, mean age = 25.8 years, SD = 5.1). Participants received $15 AUD for participation in the training session and $30 AUD for participation in the MEG session. The study was approved by the Macquarie University Human Research Ethics Committee, and all participants provided informed consent.

bioRxiv preprint doi: https://doi.org/10.1101/2021.02.28.433294; this version posted March 1, 2021. The copyright holder for this preprint (which was not certified by peer review) is the author/funder. All rights reserved. No reuse allowed without permission.

127 *2.1.2. Stimuli and experimental procedure*

128 MEG session

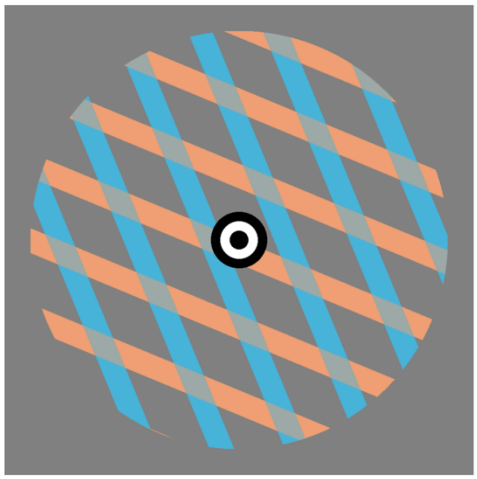
129 Participants were instructed keep fixation at a central bullseye throughout the experiment
130 and were cued to attend to either blue or orange at the start of each block (32 trials). Figure
131 1 shows the stimuli and trial procedure. First, approximately equiluminant blue and orange
132 oriented lines within a circular window were overlaid at fixation for 150ms on a mid-grey
133 background (Figure 1A). Participants attended to the lines of the cued colour, while ignoring
134 the lines of the other colour. After a 500ms blank screen, a black comparison line was
135 presented for 200ms. The task was to determine which way the cued lines had to be rotated
136 to match the orientation of the comparison line. After the comparison line was presented,
137 there was a 500ms blank screen, and then the response screen, consisting of arrows
138 showing either a clockwise or an anti-clockwise rotation, was shown until a response was
139 given. If participants did not respond within 3 seconds, the next trial started. Participants
140 pressed one of two buttons to indicate whether the rotation shown on the response screen
141 was correct or incorrect. We used this response screen to separate the correct response
142 button from the rotation direction decision, ensuring that rotation direction decoding could
143 not be driven by motor preparation. The mapping of the buttons to indicate 'correct' or
144 'incorrect' was counterbalanced across participants. Participants received feedback on every
145 trial; at the end of each trial, the white part of the fixation bullseye turned green (when
146 correct) or red (when incorrect) for 250ms to give feedback on accuracy.

147 The coloured oriented lines had a circular window of 3 degrees of visual angle
148 (DVA), a spatial frequency of 2 cycles/degree, were 2 possible colours (blue; RGB = 239,
149 159, 115 and orange; RGB = 72, 179, 217), and were phase randomised (Figure 1A). The
150 comparison line had a length of 0.8 DVA and a width of 0.1 DVA. The response mapping
151 arrows were 1.5 DVA, and the central fixation bullseye had a diameter of 0.4 DVA. There
152 were 4 possible orientations for the cued, distractor, and comparison orientations, divided

bioRxiv preprint doi: https://doi.org/10.1101/2021.02.28.433294; this version posted March 1, 2021. The copyright holder for this preprint (which was not certified by peer review) is the author/funder. All rights reserved. No reuse allowed without permission.

into 2 pairs: 22.5° was paired with 112.5°, and 67.5° was paired with 157.5° (Figure 1B). When the cued orientation was from one pair, the distractor and comparison orientation were always from the other pair. This ensured that the two overlaid orientations were never the same. The comparison orientation was always rotated 45° from the cued orientation, either in a clockwise or an anti-clockwise direction.

A



B

	Cued orientation	Distractor orientation	Rotation direction	Comparison orientation
1	22.5°	67.5°	Clockwise	67.5°
2	22.5°	67.5°	Anti-clockwise	157.5°
3	22.5°	157.5°	Clockwise	67.5°
4	22.5°	157.5°	Anti-clockwise	157.5°
5	112.5°	67.5°	Anti-clockwise	67.5°
6	112.5°	67.5°	Clockwise	157.5°
7	112.5°	157.5°	Anti-clockwise	67.5°
8	112.5°	157.5°	Clockwise	157.5°
9	67.5°	22.5°	Anti-clockwise	22.5°
10	67.5°	22.5°	Clockwise	112.5°
11	67.5°	112.5°	Anti-clockwise	22.5°
12	67.5°	112.5°	Clockwise	112.5°
13	157.5°	22.5°	Clockwise	22.5°
14	157.5°	22.5°	Anti-clockwise	112.5°
15	157.5°	112.5°	Clockwise	22.5°
16	157.5°	112.5°	Anti-clockwise	112.5°

C

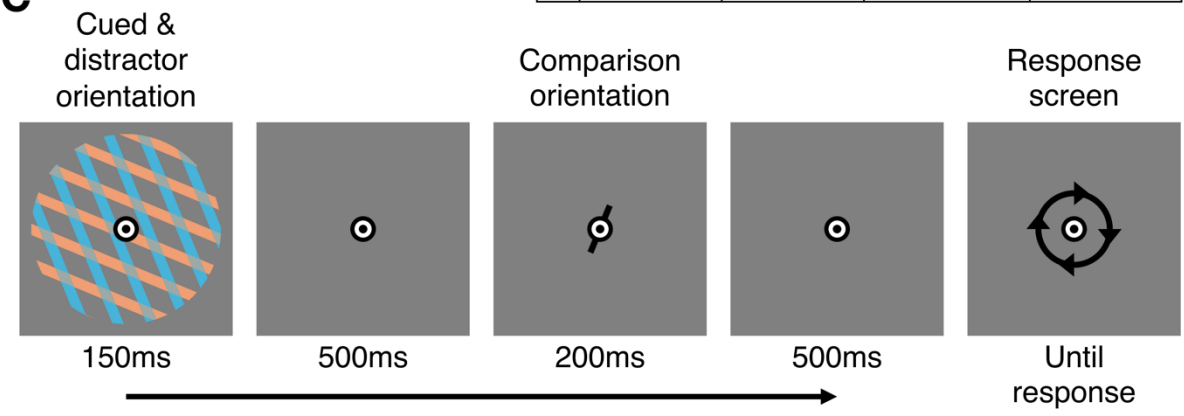


Figure 1. Stimuli and design. The stimulus, shown in **A**, consisted of oriented blue and orange lines within a circular window. Participants attended to the lines of one colour, while ignoring the lines of the other colour. **B** shows the 16 possible trial types, determined by a combination of cued orientation, distractor orientation, and rotation direction. The comparison orientation was not used in the analysis but is shown for completeness. The cued orientation, distractor orientation, and rotation direction are orthogonal dimensions in this design, only within the 2 pairs separately (top half and bottom half of the table). Decoding was done within each pair to ensure all of these factors are balanced. **C** shows an

bioRxiv preprint doi: https://doi.org/10.1101/2021.02.28.433294; this version posted March 1, 2021. The copyright holder for this preprint (which was not certified by peer review) is the author/funder. All rights reserved. No reuse allowed without permission.

example of a trial sequence. Participants were cued to a particular colour for a block of 32 trials. On each trial, the cued and distractor oriented lines were shown for 150ms followed by 500ms delay, and then the comparison orientation was shown for 200ms. After another 500ms delay, the response screen appeared until a response ('correct' vs 'incorrect') was given, or until the 3s timeout. In this trial, for example, if the cued colour was blue, the participant would have to decide whether the blue lines need to rotate clockwise or anti-clockwise to match the comparison orientation. At the response screen, which in this trial shows clockwise, the correct response would be the button indicating 'correct'.

Cued orientation (4) x distractor orientation (2) x rotation direction (2) x response screen (2) were counterbalanced within each block, and the cue colour was counterbalanced over blocks. Participants were instructed which colour to attend at the start of each block of 32 trials, and the cue colour switched between blocks. Participants completed 16 experimental runs, with 2 blocks per run (one block of 32 trials per cue colour). One participant completed 14 instead of 16 experimental runs. In addition to the feedback on every trial, participants received feedback on their accuracy at the end of each block. The order of the trial types was randomised within each block. To increase the number of correct trials, any trial on which the participant made an error was presented again later in the block. This was done a maximum of two times per block, and only if it was not the last trial in the block. We replaced error trials with successful retakes in the analysis, thus increasing the number of correct trials available for the decoding analysis. We did not record eye movements, but to influence decoding accuracy, eye-movements during the trials would have to systematically vary between the different conditions within each pair (see Figure 1B). This seems unlikely as all cued and distractor orientations were presented at fixation with no variance between conditions.

Training session

Due to the challenging task, participants completed a separate behavioural training session before doing the task in the MEG. The training session consisted of 3 parts. First, participants practiced the rotation task without selection. Only lines of the cued colour were

bioRxiv preprint doi: https://doi.org/10.1101/2021.02.28.433294; this version posted March 1, 2021. The copyright holder for this preprint (which was not certified by peer review) is the author/funder. All rights reserved. No reuse allowed without permission.

shown, and the task was slower: the cued stimulus and comparison line were both presented for 500ms instead of 150ms and 200ms respectively. Next, the selection element was introduced. Both the cued and the distractor colour lines were shown, with the timing of the task again slowed as in part 1 of the training. Finally, the task was presented at the same speed as used in the MEG session: the cued stimulus was shown for 150ms and the comparison line was presented for 200ms. Feedback was given at the end of each trial by the white part of the fixation bullseye turning green (correct) or red (incorrect) for 250ms. At the end of each block, participants also received feedback about their overall accuracy for that block.

Each run within the training session consisted of 2 blocks of 32 trials, one block per cued colour. The number of runs per training part was adjusted flexibly depending on task performance. When participants had finished at least 2 runs and achieved an average accuracy of at least 90% for the previous run, they moved onto the next part of training. Participants who were able to complete all 3 training steps within an hour-long session were invited to participate in the MEG session.

2.1.3. MEG acquisition

Participants performed the task in a supine position. The MEG signal was continuously sampled at 1000Hz on a whole-head MEG system with 160 axial gradiometers inside a magnetically shielded room (Model PQ1160R-N2, KIT, Kanazawa, Japan). All MEG recordings were obtained at the KIT-Macquarie Brain Research Laboratory, Sydney, Australia. Recordings were filtered online between 0.03Hz and 200Hz. To track head movements during the experiment, participants were fitted with a cap with 5 marker coils. We recorded the head shape of participants using a Polhemus Fastrak digitiser pen (Colchester, USA). The stimuli were projected onto the ceiling of the magnetically shielded room. To correct for delays in stimulus onsets of the projector compared to the triggers,

bioRxiv preprint doi: https://doi.org/10.1101/2021.02.28.433294; this version posted March 1, 2021. The copyright holder for this preprint (which was not certified by peer review) is the author/funder. All rights reserved. No reuse allowed without permission.

224 photodiode responses were used to determine the onset of the trial. We adjusted the stimuli
225 to correct for distortions introduced by the projector. The stimuli were presented using the
226 Psychtoolbox extension in MATLAB (Brainard, 1997; Kleiner et al., 2007; Pelli, 1997).
227 Participants used a 2-button response pad to respond on each trial.
228
229 *2.1.4. Pre-processing*
230 The data were pre-processed using the FieldTrip extension in MATLAB (Oostenveld et al.,
231 2011). The recordings were sliced into 3100ms epochs; from 100ms before the onset of the
232 first stimulus until 3000ms after stimulus onset. The signal was then down sampled to
233 200Hz. Error trials that had a successful retake were exchanged for the correct retake. To
234 keep the counterbalancing of all conditions intact, we included the few error trials that did not
235 have a successful retake in the analysis (0.33% of trials on average).
236
237 *2.1.5. Decoding analysis*
238 We used MVPA to determine whether there was information present in the pattern of
239 activation for each timepoint about: 1) the cued orientation; 2) the distractor orientation; and
240 3) the rotation direction. Comparing the coding of the cued and distractor orientations
241 allowed us to determine whether attended visual information was preferentially coded, while
242 coding of the rotation direction reflected the decision participants had to make about the
243 stimulus. Critically, the cued orientation, distractor orientation, and rotation direction were all
244 orthogonal dimensions, allowing us to investigate the coding of each of these separately.
245 For each timepoint, we trained a Support Vector Machine (SVM) classifier on the
246 activation across all 160 sensor channels to distinguish the conditions of interest. Classifier
247 performance was determined using leave-one-run-out cross-validation. Data were split into a
248 training dataset, containing the data from 15 runs, and a testing dataset, containing the data
249 from the left-out run. This was done 16 times, using a different testing run each time. The

bioRxiv preprint doi: https://doi.org/10.1101/2021.02.28.433294; this version posted March 1, 2021. The copyright holder for this preprint (which was not certified by peer review) is the author/funder. All rights reserved. No reuse allowed without permission.

250 analysis was repeated for each point in time, resulting in a decoding accuracy over time. We
251 used the CoSMoMVPA toolbox for MATLAB to conduct our MVPA analyses (Oosterhof et
252 al., 2016).

253 *Cued and distractor orientation:* To examine whether there was information about the
254 cued orientation, we trained a classifier to distinguish between the 4 possible cued
255 orientations. These 4 orientations were divided into 2 pairs (see Figure 1B); 22.5° was
256 paired with 112.5°, and 67.5° was paired with 157.5°. The classification of orientation was
257 done within each pair separately, and the decoding accuracies were then averaged over
258 pairs. This ensured that the cued orientation was orthogonal to the distractor orientation and
259 comparison orientation. For example, in pair 1, cued orientation 22.5° and 112.5° occurred
260 equally often with each of distractor orientations 67.5° and 157.5° (see Figure 1B). Cued
261 and distractor orientations were also orthogonal to the rotation decision, so that only the
262 orientation of the stimulus, and not the participant's decision about it, could drive the
263 classifier. Because the decoding was done within a pair, theoretical chance level was 50%.
264 The decoding analysis for the distractor orientation was the same, as the possible cued and
265 distractor orientations were identical.

266 *Rotation direction:* We used coding of the rotation direction as a measure for coding
267 of the decision participants had to make. To determine whether there was information about
268 the rotation direction, we trained a classifier to distinguish between a clockwise and anti-
269 clockwise rotation. The rotation direction was orthogonal to both the cued and distractor
270 orientation conditions (e.g., a clockwise decision was equally associated with all 4 possible
271 orientations). There were 2 possible rotation directions, giving a theoretical chance level of
272 50%.

273

bioRxiv preprint doi: https://doi.org/10.1101/2021.02.28.433294; this version posted March 1, 2021. The copyright holder for this preprint (which was not certified by peer review) is the author/funder. All rights reserved. No reuse allowed without permission.

274 *2.1.6. Statistics*

275 We used Bayesian statistics to determine the evidence for the coding of information under
276 the null hypothesis (chance decoding) and the alternative hypothesis (above-chance
277 decoding), for each time-point (Dienes, 2011; Jeffreys, 1998; Kass & Raftery, 1995; Rouder
278 et al., 2009; Wagenmakers, 2007), using the Bayes Factor package in R (Morey & Rouder,
279 2018). To test whether the decoding accuracy was above chance, we used a half-Cauchy
280 prior for the alternative, with the default width of 0.707 (Jeffreys, 1998; Rouder et al., 2009;
281 Wetzels et al., 2011). We used a hybrid null that combines a point null centred around
282 chance, with an interval ranging from a standardised effect size of 0 to 0.5 (Morey & Rouder,
283 2011). To test whether there was stronger information coding for the cued compared to the
284 distractor orientation, we calculated the difference between decoding accuracies for the
285 cued and distractor orientation. We used a half-Cauchy prior, centred around 0, with the
286 same width and null interval described above, for the alternative hypothesis to capture
287 directional effects (cued > distractor).

288 Bayes Factors (BFs) of <1 show evidence for the null hypothesis, while BFs of >1
289 show evidence for the alternative hypothesis. BFs between 1/3 and 3 are typically
290 interpreted as showing insufficient evidence, BFs < 1/3 or BFs >3 as substantial evidence,
291 and BFs < 1/10 or BFs >10 are interpreted as strong evidence (Wetzels et al., 2011). In this
292 study, we defined the onset of strong evidence for above-chance decoding as the second
293 consecutive timepoint with a BF >10, and the return to baseline decoding as the second
294 consecutive timepoint with a BF<1/10.

295

296 **2.2. fMRI**

297 *2.2.1. Participants*

298 The second part of the study consisted of a behavioural training session and an fMRI
299 session carried out at the MRC Cognition and Brain Sciences Unit (Cambridge, UK). 42

bioRxiv preprint doi: https://doi.org/10.1101/2021.02.28.433294; this version posted March 1, 2021. The copyright holder for this preprint (which was not certified by peer review) is the author/funder. All rights reserved. No reuse allowed without permission.

300 healthy volunteers participated in the initial training session. Of these, 27 volunteers
301 performed well enough to participate in the fMRI session (at least 90% accuracy in the final
302 run of the training session). The fMRI data from 3 participants were excluded due to
303 excessive movement, failure to complete the experiment, or low task performance (accuracy
304 < 80% in the fMRI session), resulting in a final fMRI sample of 24 participants (15 female/9
305 male, 23 righthanded/1 lefthanded, mean age = 27.33 years, SD = 5.53). One of these
306 participants also participated in the MEG experiment and 23 of the participants were new
307 recruits. Participants received £6 for participation in the training session and £20 for
308 participation in the fMRI session, as well as £2.50 - £3 travel costs per session. All
309 participants provided informed consent, and the study was approved by the Cambridge
310 Psychology Research Ethics Committee.
311
312 *2.2.2. Stimuli and experimental procedure*
313 fMRI session
314 Participants performed the same task as in the MEG, except for the following 3 changes due
315 to the lower temporal resolution of fMRI. First of all, the order of consecutive trial types was
316 not fully randomised as it was in the MEG version, but was instead counterbalanced within
317 each run, making sure each combination of cued orientation x distractor orientation x
318 comparison orientation was equally likely to follow each other combination as well as itself.
319 The order of the rotation direction was balanced separately within each run. Secondly, to
320 keep the order of consecutive trial types intact, error trials were not repeated. Thirdly,
321 participants did not receive trial-wise feedback to avoid feedback of the previous trial
322 influencing the signal of the next trial. Participants still received feedback about their
323 accuracy at the end of each block. Participants completed 8 runs, with 4 blocks per run, and
324 32 trials per block. The total number of blocks, and the number of trials per block stayed the

bioRxiv preprint doi: https://doi.org/10.1101/2021.02.28.433294; this version posted March 1, 2021. The copyright holder for this preprint (which was not certified by peer review) is the author/funder. All rights reserved. No reuse allowed without permission.

same as the MEG experiment, however, the blocks were divided into 8 runs of 4 blocks, instead of 16 runs of 2 blocks. One participant completed 7 instead of 8 runs.

Training session

The training session was the same as described in the MEG experiment section.

2.2.3. fMRI acquisition

fMRI scans were acquired using a Siemens 3 Tesla Prisma-Fit scanner (Siemens Healthcare, Erlangen, Germany), with a 32-channel head coil at the MRC Cognition and Brain Sciences Unit, Cambridge, UK. We used a multi-band T2*-weighted echo planar imaging (EPI) acquisition sequence with the following parameters: repetition time (TR) = 1208ms; echo time (TE) = 30ms; flip angle = 67 degrees, field of view = 192 mm, multi-band acceleration factor = 2, no in-plane acceleration, in-plane resolution = 3 x 3 mm, 38 interleaved slices of 3 mm slice thickness with 10% interslice gap. T1-weighted MPRAGE structural images were acquired at the start of the session (resolution = 1 x 1 x 1 mm). The stimuli were presented on a NNL LCD screen (resolution = 1920 x 1080, refresh rate = 60 Hz) using the Psychtoolbox extension in MATLAB (Brainard, 1997; Kleiner et al., 2007; Pelli, 1997). Participants used a 2-button response pad to respond on each trial. To get comfortable with performing the task in the MRI scanner, participants completed 2 practice blocks of the task during the acquisition of the structural scan at the start of the scanning session. Feedback about accuracy was given at the end of each of these practice blocks.

2.2.4. Pre-processing and first-level model

The data were pre-processed using SPM 8 (Wellcome Department of Imaging Neuroscience) in MATLAB. EPI images were converted to NIFTII format, spatially realigned to the first image and slice-time-corrected (slice timing correction used the routine from

bioRxiv preprint doi: https://doi.org/10.1101/2021.02.28.433294; this version posted March 1, 2021. The copyright holder for this preprint (which was not certified by peer review) is the author/funder. All rights reserved. No reuse allowed without permission.

SPM12 to allow for multiband acquisitions). Structural scans were co-registered to the mean EPI image and normalised to derive the normalisation parameters needed for the definition of the regions of interest (ROIs).

To obtain activation patterns for the MVPA analysis, we estimated a General Linear Model (GLM) for each participant. There were 16 regressors per run, reflecting a combination of 4 cued orientations x 2 distractor orientations x 2 rotation directions (see Figure 1B). Whole trials were modelled as a single events, lasting from the onset of the first stimulus until the response was given, to account for trial-to-trial variability in response time (Woolgar et al., 2014). Regressors were convolved with the hemodynamic response function of SPM8.

2.2.5. Regions of interest

13 frontal and parietal MD ROIs were taken from the parcellated map provided by Fedorenko et al (2013), which is freely available online at imaging.mrc-cbu.cam.ac.uk/imaging/MDsystem. The definition of the MD network is activation based, as the map indexes regions that show a univariate increase in activation with increased task demands, across a range of tasks. This is an updated definition of the MD system, with a high degree of overlap with the previous definition, derived from meta-analytic data (Duncan & Owen, 2000) that we used in previous work (Jackson et al., 2016; Jackson & Woolgar, 2018; Woolgar, Williams, et al., 2015; Woolgar, Afshar, et al., 2015), and a more recent definition derived from multimodal imaging (Assem et al., 2020). The ROIs comprised left and right anterior inferior frontal sulcus (aIFS; center of mass (COM) = ±35 47 19, volume = 5.0 cm^3), left and right posterior inferior frontal sulcus (pIFS; COM ±40 32 27, 5.7 cm^3), left and right premotor cortex (PM; COM ±28 –2 56, 9.0 cm^3), left and right inferior frontal junction (IFJ; COM ±44 4 32, 10.1 cm^3), left and right anterior insula/frontal operculum (AI/FO; COM ±34 19 2, 7.9 cm^3), left and right intraparietal sulcus (IPS; COM ±29 –56 46,

bioRxiv preprint doi: https://doi.org/10.1101/2021.02.28.433294; this version posted March 1, 2021. The copyright holder for this preprint (which was not certified by peer review) is the author/funder. All rights reserved. No reuse allowed without permission.

377 34.0 cm^3), and bilateral anterior cingulate cortex (ACC; COM 0 15 46, 18.6 cm^3). Early visual
378 cortex was defined as area BA 17 (center of mass = −13, −81, 3/16, −79, 3, volume = 54
379 cm^3) from the Brodmann template provided with MRIcro (Rorden & Brett, 2000). ROIs were
380 deformed into native space by applying the inverse of the normalisation parameters for each
381 participant.
382
383 *2.2.6. Decoding analysis*
384 We used the same decoding analysis as described in the MEG experiment but in the MEG
385 experiment, we used MVPA to determine what information is present in the pattern of
386 activation for each *point in time*, whereas for the fMRI data, we determine what information
387 is present in the pattern of activation *for each ROI*. Within each ROI, we trained an SVM
388 classifier on the betas obtained from the GLM to distinguish the conditions of interest. The
389 classifier performance was determined by using a leave-one-run-out cross-validation.
390 Decoding accuracies were then averaged over hemispheres.
391
392 *2.2.7. Statistics*
393 To test for an effect of attention, MD region, and the interaction between these factors, we
394 used a Bayesian analysis of variance (ANOVA) with attention (cued vs. distractor
395 orientation) and MD region (aIFS, pIFS, PM, IFJ, AI/FO, IPS, and ACC; data collapsed
396 across hemispheres) as within-subject factors, using the default Jeffries prior of medium
397 width (1/2) (Rouder et al., 2012). We conducted further Bayesian t-tests using the same
398 parameters described in the MEG experiment. To determine the contribution of individual
399 MD regions and V1 to the effect of attention on stimulus coding, we performed Bayesian
400 tests of the difference between decoding of the cued and distractor orientation per MD ROI
401 and V1. In addition, we performed Bayesian tests for the decoding of the cued orientation,
402 distractor orientation, and rotation direction against chance for the mean MD regions, per

bioRxiv preprint doi: https://doi.org/10.1101/2021.02.28.433294; this version posted March 1, 2021. The copyright holder for this preprint (which was not certified by peer review) is the author/funder. All rights reserved. No reuse allowed without permission.

individual MD region and for V1. We used the same parameters for these tests as described in the MEG section (2.1.6).

2.3. Model-based MEG-fMRI fusion

To gain insight into the coding of attended information, unattended information, and decision-related information in both space and time simultaneously, we used model-based MEG-fMRI fusion (Cichy et al., 2014, 2016; Hebart et al., 2018). This method uses Representational Dissimilarity Matrices (RDMs) (Kriegeskorte et al., 2006, 2008) to abstract away from the imaging modality, allowing us to compare the pattern similarity across neuroimaging modalities. Model-based MEG-fMRI fusion further allows us to determine the match between the representational structure for each timepoint (MEG), and each ROI (fMRI), which can be uniquely explained by a theoretical model (Hebart et al., 2018) (see Figure 6A for an overview of this method). We used 3 orthogonal models, coding for the *cued orientation*, *distractor orientation*, and *rotation direction*.

The RDMs consisted of a 16 by 16 matrix comprising each combination of cued orientation (4) x distractor orientation (2) x rotation direction (2) (see Figure 1B for an overview of combinations). For each cell in the RDM, we used decoding accuracy as our measure of dissimilarity, with greater decoding accuracy reflecting greater dissimilarity of activation patterns (i.e., distinctiveness of patterns between the conditions). Decoding accuracies were obtained for each cell in the RDM (i.e., pair of trial types) using the same cross-validation procedure as described above and were z-scored per ROI and timepoint. For the MEG data, we constructed an RDM at each timepoint. For each cell in the RDM, we obtained decoding accuracies using a 25ms sliding window centred around each timepoint. For the fMRI data, we constructed an RDM for the mean MD and V1 ROIs. The mean MD ROI was obtained by calculating the RDM for each individual MD region and averaging

bioRxiv preprint doi: https://doi.org/10.1101/2021.02.28.433294; this version posted March 1, 2021. The copyright holder for this preprint (which was not certified by peer review) is the author/funder. All rights reserved. No reuse allowed without permission.

428 across regions[1]. We did this separately for each participant, and then averaged the RDMs
429 over participants, resulting in a single RDM per timepoint for MEG, and per ROI for fMRI. We
430 constructed 3 model RDMs: for the cued orientation, distractor orientation, and rotation
431 direction (see Figure 6A). The cued and distractor orientation models coded for: the same
432 orientation (0), a difference of 45° (0.5), or a difference of 90° (1); the rotation direction
433 model coded for the same rotation (0) or a different rotation (1).
434 We used commonality analysis to estimate the shared variance between 3 RDMs:
435 the MEG RDM for each point in time, the fMRI RDM for each ROI, and the model RDM. For
436 each timepoint, ROI, and model, we calculated the difference between two squared semi-
437 partial correlation coefficients, using Spearman correlation. Both semi-partial correlation
438 coefficients reflected the proportion of variance shared between MEG and fMRI; one with *all*
439 *models* partialled out from the MEG RDM, and the other with *all models except the model of*
440 *interest* partialled out from the MEG RDM. By comparing the variance when our model of
441 interest was included or not, we get a measure of the variance shared between MEG and
442 fMRI that can be uniquely explained by each model (Hebart et al., 2018). In this way we
443 derive a time-course of the model fit for each region.
444
445 *2.3.1. Statistics*
446 Because we averaged the RDMs over participants for both MEG and fMRI, we had a single
447 RDM for each timepoint for MEG, and a single RDM for each ROI for fMRI. To estimate the
448 null distribution, we computed 10,000 permutations by shuffling the rows and columns of the
449 group average MEG RDM and ran model-based MEG-fMRI fusion for each ROI using the
450 permuted MEG matrices. For each ROI, we then determined a cluster-inducing threshold for
451 each timepoint by choosing the 95th percentile. We determined the largest maximum cluster

[1] We could instead have calculated the RDM by extracting the data from one large ROI including all MD regions; in practice this gave a similar RDM so was not considered further.

bioRxiv preprint doi: https://doi.org/10.1101/2021.02.28.433294; this version posted March 1, 2021. The copyright holder for this preprint (which was not certified by peer review) is the author/funder. All rights reserved. No reuse allowed without permission.

size in the null distribution. We did this over both ROIs to account for multiple comparisons over our 2 ROIs. We compared the clusters in our fusion data to the maximum cluster size obtained from the null distribution (equivalent to $p<0.05$, one-tailed, corrected for multiple comparisons for the two ROIs and all the timepoints).

3. RESULTS

3.1. MEG results

3.1.1. Behavioural results for MEG session

Participants performed with high accuracy in the MEG session. The mean accuracy was 94.23% (SD = 3.90) before replacing error trials (see Methods), and 99.67% (SD = 0.56) after replacing error trials where possible, which means very few error trials were included in the analysis (0.33% of trials on average). The mean response time was 667ms (SD = 104ms).

3.1.2. Coding of the cued and distractor orientation over time

To examine the timepoints at which attended visual information was preferentially coded over unattended visual information, we compared the decoding accuracies for the same orientations when presented as the cued or distractor orientation for each point in time. Critically, the coding of the cued and distractor information could not be driven by decision-related information, as this was an orthogonal dimension in the design. The decoding accuracies for the cued and distractor orientations are shown in Figure 2. There was strong evidence for above-chance orientation decoding for the cued orientation starting at 85ms after stimulus onset, which was maintained until after the mean response time. The distractor stimulus orientation could be decoded with a very similar onset to the cued orientation, with strong evidence for above-chance coding from 90ms after stimulus onset. However, unlike the coding of the cued information, coding of the distractor orientation was

bioRxiv preprint doi: https://doi.org/10.1101/2021.02.28.433294; this version posted March 1, 2021. The copyright holder for this preprint (which was not certified by peer review) is the author/funder. All rights reserved. No reuse allowed without permission.

not sustained over time, dropping back to chance within 420ms after stimulus onset. The difference between coding of the cued and distractor orientations, which reflects the attentional selection and maintenance of task-relevant information, was evident from 215ms after stimulus onset. This effect of attention, with stronger coding of the cued compared to distractor orientation, was maintained until after the mean response time.

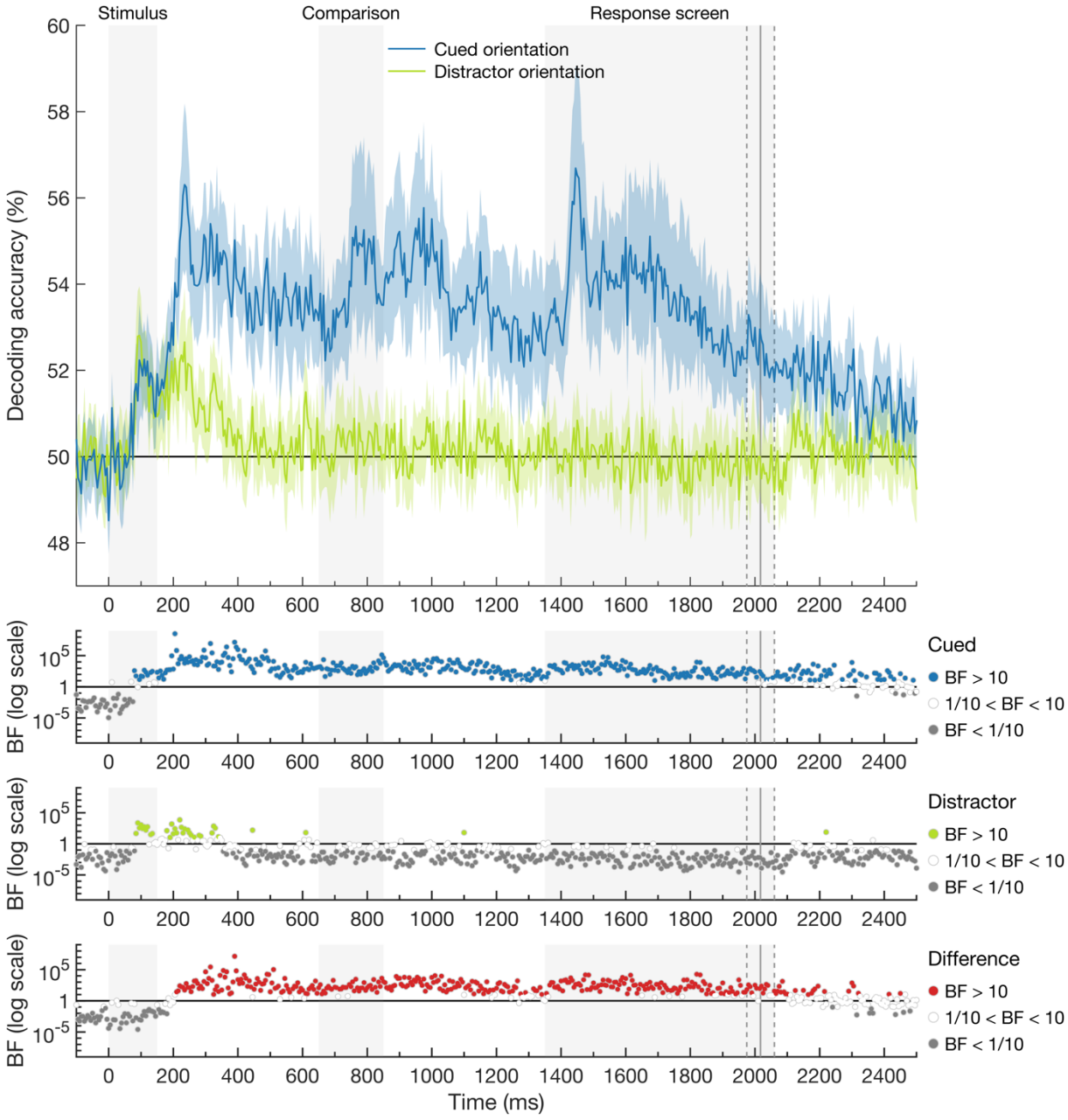


Figure 2. Decoding accuracy of the cued and distractor orientation over time. Classifiers were trained to discriminate stimulus orientation when the orientation was either cued (blue) or not (light green). Theoretical chance is 50% decoding accuracy, and shaded

bioRxiv preprint doi: https://doi.org/10.1101/2021.02.28.433294; this version posted March 1, 2021. The copyright holder for this preprint (which was not certified by peer review) is the author/funder. All rights reserved. No reuse allowed without permission.

areas around the plot lines show the 95% confidence intervals. The grey shaded areas show from left to right: 1) when the stimulus was on the screen (oriented lines in cued and distractor colours; labelled Stimulus), 2) when the comparison line was on the screen (labelled Comparison), and 3) when the response screen was shown (labelled Response screen). The response screen remained on until participants responded (or 3secs). The vertical grey lines show the mean response time with 95% confidence intervals. Bayes factors are given below the plot on a logarithmic scale for the cued orientation (blue), the distractor orientation (light green) and the difference between the cued and distractor orientation (red). BFs below 1/10 are shown in grey, indicating strong evidence for the null hypothesis. BFs above 10 are shown in the plot colour (blue for the cued orientation, light green for the distractor orientation, and red for the effect of attention), indicating strong evidence for the alternative hypothesis. BF between 1/10 and 10 are shown in white. There was strong evidence for coding of the cued orientation from 85ms after the onset of the stimulus which was maintained until after the response was given. There was strong evidence for coding of the distractor orientation from 90ms after the onset of the stimulus, but this was not sustained over time. There was strong evidence for an effect of attention from 215ms after the onset of the stimulus until after the mean response time.

3.1.3. Coding of the rotation direction over time

To examine the time-course of decision-related information coding, we determined the coding of the rotation direction over time by training a linear classifier to distinguish between clockwise and anti-clockwise rotations. Participants had to actively manipulate the cued orientation in combination with the comparison orientation to determine the rotation. The decoding of the rotation direction over time is shown in Figure 3. We observed above-chance decoding of the rotation direction from 170ms after the onset of the comparison line, 820ms after the onset of the attended and unattended orientations, which was maintained until after the mean response time.

bioRxiv preprint doi: https://doi.org/10.1101/2021.02.28.433294; this version posted March 1, 2021. The copyright holder for this preprint (which was not certified by peer review) is the author/funder. All rights reserved. No reuse allowed without permission.

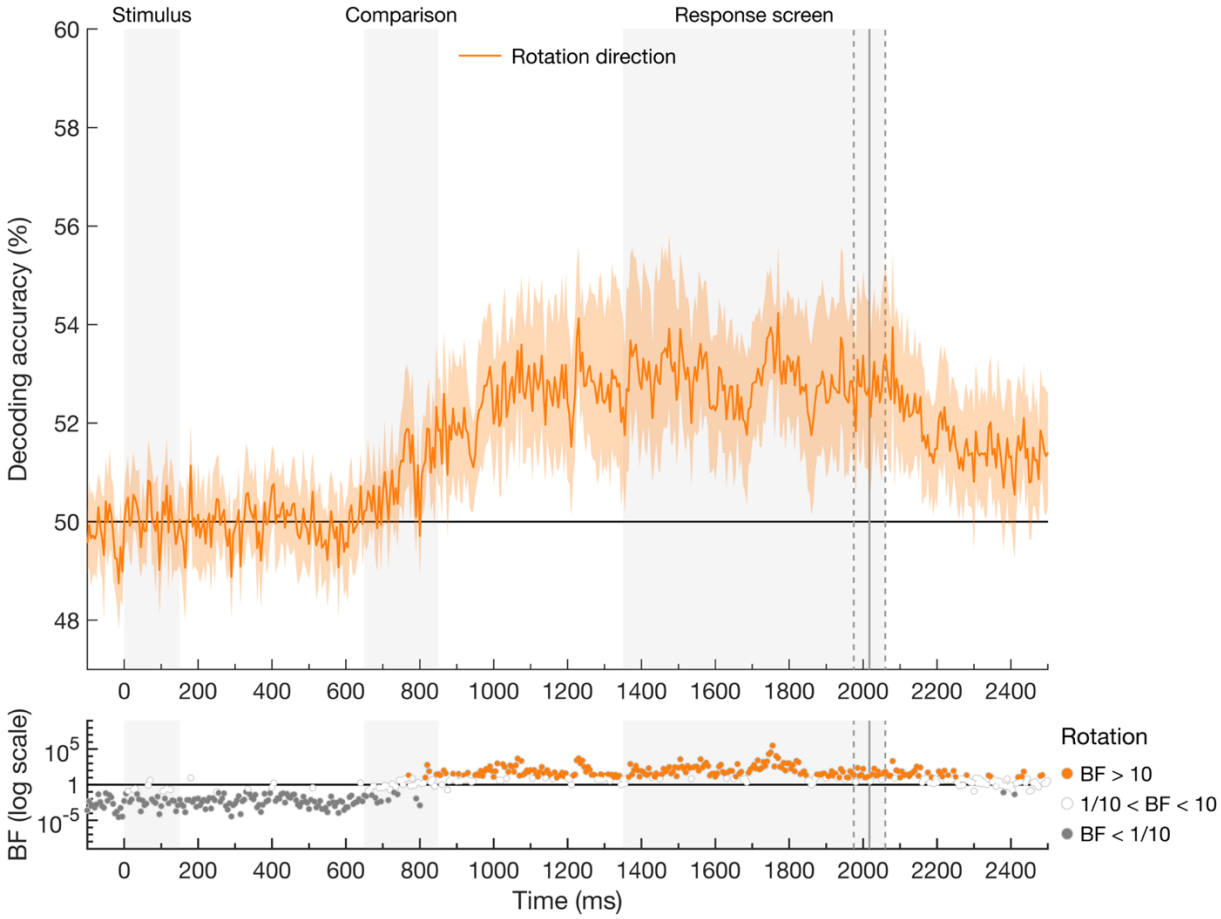


Figure 3. Decoding accuracy of the rotation direction over time. Classifiers were trained to discriminate the rotation direction, which could be clockwise or anti-clockwise. The rotation direction, about which participants had to make a decision, could be decoded from 170ms after the onset of the comparison line (820ms after stimulus onset) and was maintained until after the mean response time. Plotting conventions are as in Figure 2.

3.2. fMRI results

3.2.1. Behavioural results for fMRI session

Participants performed the task in the fMRI session with high accuracy (mean accuracy = 94.45%, SD = 4.91). Included participants all had a mean accuracy above 80%. The mean response time was 658ms (SD = 140ms) from response screen onset.

3.2.2. Coding of the cued and distractor orientation in the MD regions and V1

To examine whether the effect of attention observed in the MEG data pertained to V1 and the MD regions, we decoded the cued and distractor orientations for these ROIs. We were

bioRxiv preprint doi: https://doi.org/10.1101/2021.02.28.433294; this version posted March 1, 2021. The copyright holder for this preprint (which was not certified by peer review) is the author/funder. All rights reserved. No reuse allowed without permission.

able to separate these conditions due to the orthogonal design. The decoding accuracies for the cued and distractor orientations, averaged across the MD regions and in V1, are shown in Figure 4A. We used a Bayesian ANOVA with attention (orientation coding of cued vs. distractor stimuli) and MD region (aIFS, pIFS, PM, IFJ, AI/FO, IPS, and ACC; data collapsed across hemispheres) as within-subject factors. We found a main effect of attention (BF > 100), but there was not enough evidence for a main effect of region (BF = 0.44). There was evidence for an interaction between attention and region (BF = 9.60) justifying a further analysis of the effect of attention in individual MD regions (see Figure 4B). There was strong evidence for an effect of attention (cued > distractor coding) in aIFS, pIFS, PM, IFJ, and IPS, and some evidence for an effect of attention in AI/FO and ACC (see Figure 4B).

To determine whether the orientation coding for the cued and distractor orientations was above chance, we performed Bayesian t-tests for the mean MD regions as well as the individual MD regions. There was strong evidence for above-chance coding for the cued orientation in the mean MD regions (mean accuracy = 55.62%, BF > 100), while decoding of the distractor orientation was at chance (mean accuracy = 49.56%, BF < 0.01). There was above-chance decoding for the cued orientation in all of the MD regions. Strong evidence for chance level decoding for the distractor orientation was found for aIFS, pIFS, PM, IFJ, AI/FO, and IPS. There was some evidence for chance decoding for the distractor orientation in ACC, and the 95% confidence intervals for this region overlapped with chance.

We also found an effect of attention in V1 (BF > 100), with stronger coding for the cued orientations compared to the distractor orientations. V1 coded for the cued orientation (mean accuracy = 66.34%, BF>100), while there was no evidence for coding of the identical orientations when they were distractors. There was some evidence for chance decoding of the distractor orientation in V1 (mean accuracy = 51.29%, BF = 0.28), and the 95% confidence intervals overlapped with chance.

bioRxiv preprint doi: https://doi.org/10.1101/2021.02.28.433294; this version posted March 1, 2021. The copyright holder for this preprint (which was not certified by peer review) is the author/funder. All rights reserved. No reuse allowed without permission.

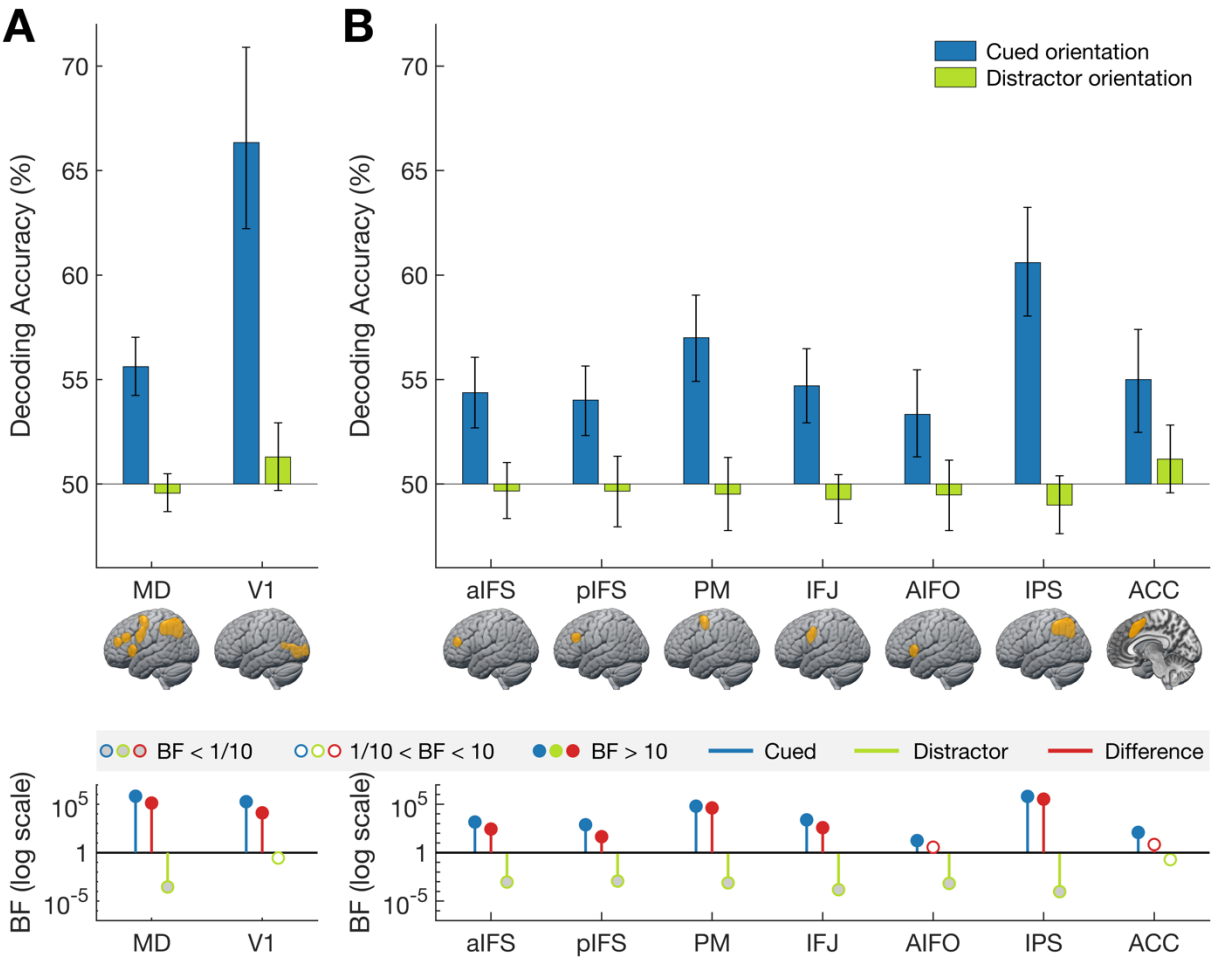


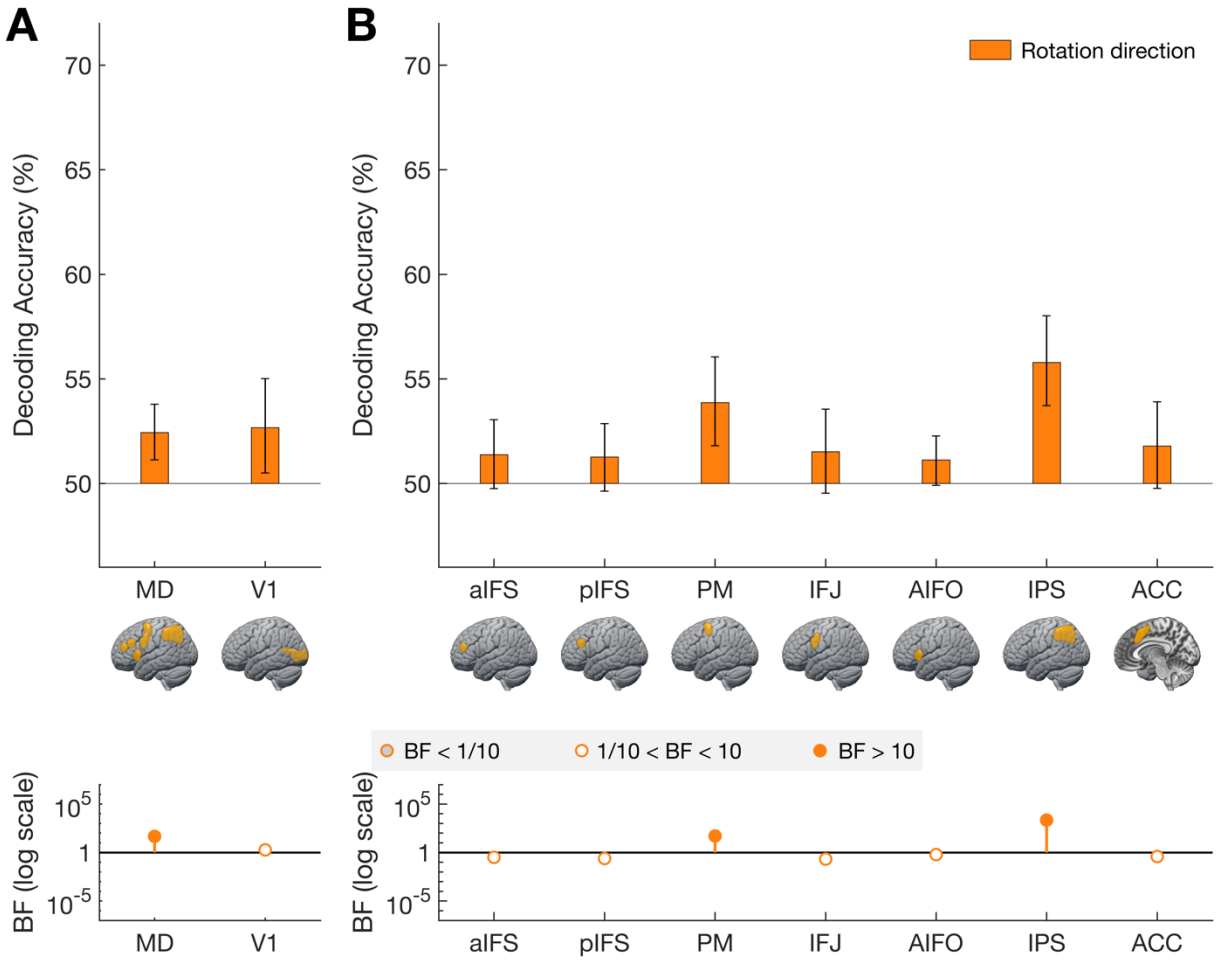
Figure 4. Decoding accuracy of the cued and distractor orientation (A) averaged across the MD regions and in V1; and (B) in individual MD regions. In both **A** and **B**, classifiers were trained to discriminate stimulus orientation when the orientation was either cued (blue) or not (light green). Theoretical chance is 50%, and error bars indicate 95% confidence intervals. The Bayes factors for the decoding accuracies are shown below the plot in blue (cued orientation) and light green (distractor orientation), and the BFs for the difference (cued>distractor coding) are shown in red. All BFs are shown on a logarithmic scale. BFs > 10 are marked in the plot colour, BFs < 1/10 are marked in grey, and BFs in between this range are marked in white. In all of the MD regions, and in V1, there was strong evidence for coding of the cued orientation, but not for the distractor orientation. There was strong evidence for an effect of attention for most of the MD regions (aIFS, pIFS, PM, IFJ, AI/FO, and IPS) as well as average MD and V1.

3.2.3. Coding of the rotation direction in the MD regions and V1

To examine whether there was information about the rotation direction, which is our indicator of the decision, in the MD regions and V1, we trained a linear classifier to distinguish between a clockwise and anti-clockwise rotation direction. Since error trials were included in the analysis to maintain the orthogonality of the different features, the decoded rotation

bioRxiv preprint doi: https://doi.org/10.1101/2021.02.28.433294; this version posted March 1, 2021. The copyright holder for this preprint (which was not certified by peer review) is the author/funder. All rights reserved. No reuse allowed without permission.

direction on these trials does not always reflect the decision of the participant. However, as this only occurred on ~6% of trials, the predominant influence will be the decision. Figure 5A shows the decoding accuracies for the rotation direction in the MD regions and V1. We used Bayesian t-tests to determine the evidence for chance versus above-chance decoding. We observed strong evidence for above-chance coding of rotation direction across the MD regions on average (mean accuracy = 52.43%, BF = 45.89), and in PM and IPS individually (Figure 5B). Although the average decoding accuracy found in V1 was similar to the MD regions, greater variance in V1 was reflected in an inconclusive BF (mean accuracy = 52.67%, BF = 1.85). There was substantial, but not strong, evidence for chance decoding in aIFS, pIFS, and IFJ, and insufficient evidence for rotation direction coding in the other MD regions.



bioRxiv preprint doi: https://doi.org/10.1101/2021.02.28.433294; this version posted March 1, 2021. The copyright holder for this preprint (which was not certified by peer review) is the author/funder. All rights reserved. No reuse allowed without permission.

Figure 5. Decoding accuracy of the rotation direction (decision) (A) averaged across the MD regions and in V1 and (B) in individual MD regions. In both **A** and **B**, classifiers were trained to discriminate the rotation direction, which could be clockwise or anti-clockwise. Plotting conventions are as in Figure 4. The rotation direction could be decoded from the MD regions (average, PM and IPS), while there was insufficient information for rotation direction coding in V1.

3.3. Model-based MEG-fMRI fusion results

We used model-based MEG-fMRI fusion to investigate whether the MD regions code attended information *before* a decision is made (see Figure 6A). Figure 6B and 6C show the commonality coefficient over time for our 2 ROIs: the MD regions and V1. The commonality refers to the part of the variance that is shared between the MEG and fMRI RDMs, which can be uniquely explained by our models for the cued orientation, distractor orientation, and rotation direction.

3.3.1. Cued orientation

In the MD regions, there was a significant cluster of commonality for the cued orientation from 555ms until 640ms after the onset of the stimulus (Figure 6B). Critically, this cluster occurred *before* the onset of the comparison line, and therefore before participants could make the decision. A second cluster started at 1140ms, 490ms after the onset of the comparison line and was maintained until after the average response time. In V1, cued orientation commonality coefficients were significant from 225ms until 505ms after the onset of the stimulus, and again from 1210ms, 560ms after the onset of the comparison line, until after the mean response time (Figure 6C).

3.3.2. Distractor orientation

There were no significant clusters of commonality for the distractor orientation in the MD region or V1.

bioRxiv preprint doi: https://doi.org/10.1101/2021.02.28.433294; this version posted March 1, 2021. The copyright holder for this preprint (which was not certified by peer review) is the author/funder. All rights reserved. No reuse allowed without permission.

3.3.3. Rotation direction

We observed a cluster of significant commonality for the rotation direction, which is an index of the decision participants had to make, in the MD regions starting from 1140ms, 490ms after the onset of the comparison line, which lasted until after the participant responded. V1 showed a similar pattern over time, with a significant rotation direction cluster from 1160ms, 510ms after comparison line onset.

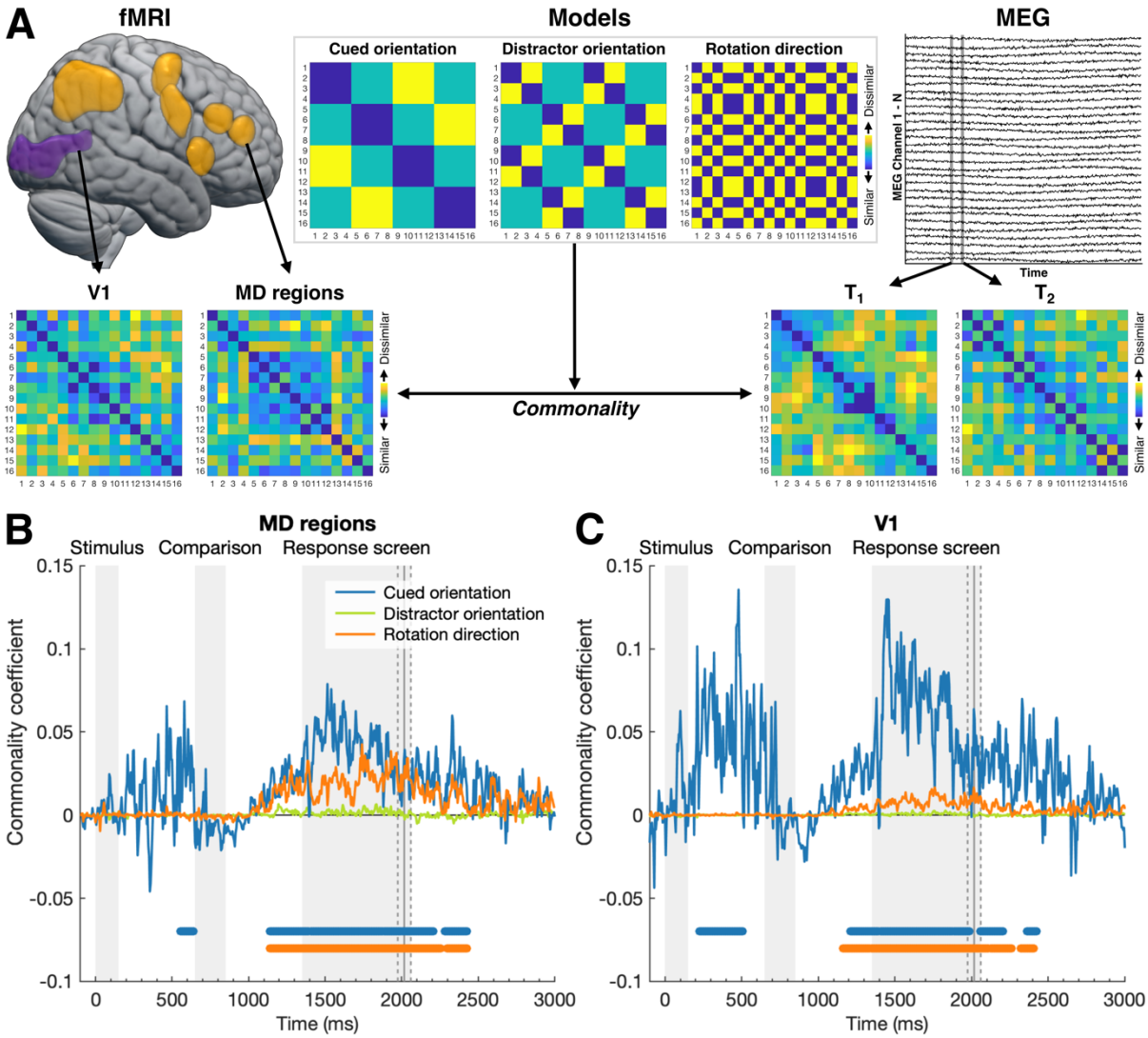


Figure 6. Model-based MEG – fMRI fusion methods (A) and results over time for the MD regions (B) and V1 (C). **A** gives an overview of the model-based MEG – fMRI fusion method. We used RDMs to abstract away from the imaging modality. Each cell in the RDM corresponds to the dissimilarity between 2 specific trial types. A trial type is a combination of the cued orientation, distractor orientation, and rotation direction. Trial types 1-16 in the RDMs correspond to the 16 trial types listed in Figure 1B. We created an RDM for each region of interest (V1 and mean MD regions) for the fMRI data, for each time-point in the

bioRxiv preprint doi: https://doi.org/10.1101/2021.02.28.433294; this version posted March 1, 2021. The copyright holder for this preprint (which was not certified by peer review) is the author/funder. All rights reserved. No reuse allowed without permission.

MEG data, and for the 3 models (cued orientation, distractor orientation, and rotation direction). We then determined commonality: the part of the variance that is shared between the MEG RDM for each timepoint and the fMRI RDM for each ROI, that can be uniquely explained by each theoretical model. This results in a time-course of commonality coefficients for each ROI and model. **B** and **C** show the time-course of commonality for the MD regions and V1 respectively. The different lines depict the commonality explained by the model for the cued orientation (blue), the distractor orientation (light green), and the rotation direction (orange). Significant timepoints (equivalent to $p<0.05$, one-tailed) were obtained with a cluster-corrected randomisation test, corrected for multiple comparisons across ROIs and timepoints, and are shown at the bottom of the plots. Plotting conventions are as in Figure 2 and 3 except that the dots in the bottom of this plot show significant time-points, not Bayes Factors.

4. DISCUSSION

A wealth of fMRI, MEG and non-human primate studies have shown preferential coding of cued compared to distractor information (Bode & Haynes, 2009; Goddard et al., 2019; Harel et al., 2014; Jackson et al., 2016; Li et al., 2007; Rao et al., 1997; Sigala et al., 2008; Stiers et al., 2010; Stokes et al., 2013; Waskom et al., 2014; Woolgar, Afshar, et al., 2015; Woolgar, Hampshire, et al., 2011; Woolgar, Thompson, et al., 2011; Woolgar, Williams, et al., 2015). However, many paradigms manipulate attention by asking participants to respond to the cued (but not the distractor) stimulus, which means they cannot distinguish between preferential coding of cued information due to attentional selection and maintenance of relevant information, and coding due to decision-making processes performed on the attended information. We used MEG, fMRI, and model-based MEG-fMRI fusion to distinguish between these explanations. Our MEG data showed that attention affects stimulus processing around 215ms after stimulus onset, before participants had the necessary information to make a decision. Then, when the comparison line was presented, the decision about the rotation direction could be decoded approximately 170ms later. Our fMRI data showed the MD regions coded attended visual information, and did so more strongly than distracting visual information, even though the decision to be made was orthogonal to the stimulus itself. The orthogonal decision representation was also present in

bioRxiv preprint doi: https://doi.org/10.1101/2021.02.28.433294; this version posted March 1, 2021. The copyright holder for this preprint (which was not certified by peer review) is the author/funder. All rights reserved. No reuse allowed without permission.

the MD system, specifically in PM and IPS. We also found an effect of attention in V1, with stronger coding of the cued compared to distractor orientations, in line with previous studies (Jackson et al., 2016; Jehee et al., 2012; Pratte et al., 2013; Woolgar, Hampshire, et al., 2011). Our model-based MEG-fMRI fusion analysis showed evidence for the coding of attended orientation information in the MD regions *before* participants could make a decision. These data are consistent with the interpretation of previous results as effects of attention on the processing of visual stimuli, with a stronger coding of attended compared to unattended visual information in the brain. This could be driven by an enhancement of the attended visual information, a suppression of the unattended visual information, or both.

The finding that the MD regions preferentially code for attended information over unattended information, even when the decision is orthogonal, is in line with the finding of Hon and colleagues (2006), who used univariate analyses to show that the average MD response reflected changes in cued information when no decision was needed, or when the decision was unrelated to the cued information. Our results take the inference beyond simple activation changes and confirm that decision-making processes are not required for the prioritisation of cued over distractor information.

Our results also show that, in addition to coding the attended information, MD regions also code for decision-related information. The PM and IPS, which are part of the MD network, held information about the rotation direction, which participants had to make a decision about. The time-course with which this information emerged, from about 170ms after the onset of the comparison line, fits well with a previous study which found a perceptual decision on a pure noise image could be decoded around 140-180ms (Bode et al., 2012). The fast time-course suggests the coding of rotation direction information could reflect the accumulation of decision-related information, before the participant is able to respond. This is in line with the description of decision-making as the accumulation of evidence towards one of two decision alternatives until a decision boundary is reached (Gold

bioRxiv preprint doi: https://doi.org/10.1101/2021.02.28.433294; this version posted March 1, 2021. The copyright holder for this preprint (which was not certified by peer review) is the author/funder. All rights reserved. No reuse allowed without permission.

691 & Shadlen, 2007; Heekeren et al., 2008; Ratcliff & McKoon, 2007). However, we cannot
692 comment on the exact delay between the onset of decision information coding and the
693 response, as our task involved a delayed response - participants could only respond after
694 the response screen came on.

695 In addition to separating the effects of attention and decision-making, our study adds
696 to the literature by combining neuroimaging techniques, giving us resolution in both space
697 and time for a single paradigm. Our MEG data show that the effect of attention emerges
698 *before* participants have all of the information needed to make a decision, while our fMRI
699 data show that the MD regions code both attended visual information and the decision
700 participants have to make about the stimulus. Moreover, we formally related the two results
701 using model-based MEG-fMRI fusion in order to estimate the time-course of response in the
702 MD network and V1 separately. The data suggest that visual information arises first in V1,
703 but that both V1 and the MD regions code for information about the attended orientation
704 *before* participants can begin to make a decision. Orthogonal decision-related signals in MD
705 cortex arose only after the comparison line was presented. The MEG-fMRI fusion method is
706 an exciting step towards resolving neural processes in both time and space, but is limited in
707 sensitivity since it is only able to pick up effects that are present in both the MEG data and
708 the fMRI data (see Cichy & Oliva (2020) for an overview of possible limitations). For
709 instance, although our MEG data revealed transient coding of unattended information, this
710 was not evident in the fusion results, presumably because the much slower time resolution
711 of fMRI obscured its detection. This highlights the utility of considering the data from each
712 neuroimaging technique separately, as well as together.

713 Our findings emphasise the adaptable response of the MD regions, in line with the
714 literature in non-human primates showing the same neural populations can simultaneously
715 encode multiple task parameters (Aoi et al., 2020; Fusi et al., 2016; Rigotti et al., 2013). For
716 example, Aoi and colleagues (2020) show that a single neural population in monkey

bioRxiv preprint doi: https://doi.org/10.1101/2021.02.28.433294; this version posted March 1, 2021. The copyright holder for this preprint (which was not certified by peer review) is the author/funder. All rights reserved. No reuse allowed without permission.

prefrontal cortex can maintain information about relevant and irrelevant sensory information, as well as the saccade response, over the course of a trial. Our study also provides evidence for a multi-faceted response of the MD regions, although we cannot determine whether this is driven by the same population of neurons within those brain areas. The flexible MD response observed in our study, reflecting relevant visual information as well as decisions about this information, is consistent with the proposal that these regions play a key role in associating different types of information by integrating information over multiple sources (Duncan, et al., 2020). The MD system is well placed to achieve this, being widely distributed and strongly interconnected across the cortex (Assem et al., 2020; Duncan et al., 2020). In addition, our results emphasise an explicit role of the MD regions in selective attention, with preferential coding of the information that is task relevant separately from functional decisions.

In summary, our MEG results show that attention affects the representation of visual stimuli in advance of decision-making processes, while the fMRI results show that the MD regions code for attended visual information as well as decisions about this information. The MEG-fMRI fusion results show the spatio-temporal unfolding of these processes, suggesting that the MD regions represent information about the attended stimulus before participants can begin to make a decision. These results emphasise a key role for the MD regions in selective attention and are consistent with the proposal that these regions integrate different types of information for decision-making. Our multimodal data demonstrate that selective attention and decision-making have separable bases in neural coding.

5. ACKNOWLEDGEMENTS

This work was supported by the Australian Research Council (ARC) Centre of Excellence in Cognition and its Disorders (CE110001021), International Research Training Program Scholarships from Macquarie University awarded to DM, an ARC Discovery Project

bioRxiv preprint doi: https://doi.org/10.1101/2021.02.28.433294; this version posted March 1, 2021. The copyright holder for this preprint (which was not certified by peer review) is the author/funder. All rights reserved. No reuse allowed without permission.

743 (DP170101840) awarded to ANR and AW, and by the Medical Research Council (UK)
744 intramural funding (SUAG/052/G101400) awarded to AW.

745

746 **6. REFERENCES**

747 Aoi, M. C., Mante, V., & Pillow, J. W. (2020). Prefrontal cortex exhibits multidimensional
748 dynamic encoding during decision-making. *Nature Neuroscience*, *23*(11), 1410–
749 1420. https://doi.org/10.1038/s41593-020-0696-5

750 Assem, M., Glasser, M. F., Van Essen, D. C., & Duncan, J. (2020). A Domain-General
751 Cognitive Core Defined in Multimodally Parcellated Human Cortex. *Cerebral Cortex*,
752 *30*(8), 4361–4380. https://doi.org/10.1093/cercor/bhaa023

753 Battistoni, E., Kaiser, D., Hickey, C., & Peelen, M. V. (2018). Spatial attention follows
754 category-based attention during naturalistic visual search: evidence from MEG
755 decoding. *BioRxiv*, 390807. https://doi.org/10.1101/390807

756 Bode, S., & Haynes, J.-D. (2009). Decoding sequential stages of task preparation in the
757 human brain. *NeuroImage*, *45*(2), 606–613.
758 https://doi.org/10.1016/j.neuroimage.2008.11.031

759 Bode, S., Sewell, D. K., Lilburn, S., Forte, J. D., Smith, P. L., & Stahl, J. (2012). Predicting
760 Perceptual Decision Biases from Early Brain Activity. *Journal of Neuroscience*,
761 *32*(36), 12488–12498. https://doi.org/10.1523/JNEUROSCI.1708-12.2012

762 Brainard, D. H. (1997). The Psychophysics Toolbox. *Spatial Vision*, *10*(4), 433–436.
763 https://doi.org/10.1163/156856897X00357

764 Carrasco, M. (2011). Visual attention: The past 25 years. *Vision Research*, *51*(13), 1484–
765 1525. https://doi.org/10.1016/j.visres.2011.04.012

766 Cichy, Radoslaw M., & Oliva, A. (2020). A M/EEG-fMRI Fusion Primer: Resolving Human
767 Brain Responses in Space and Time. *Neuron*, S0896627320305183.
768 https://doi.org/10.1016/j.neuron.2020.07.001

bioRxiv preprint doi: https://doi.org/10.1101/2021.02.28.433294; this version posted March 1, 2021. The copyright holder for this preprint (which was not certified by peer review) is the author/funder. All rights reserved. No reuse allowed without permission.

769 Cichy, Radoslaw Martin, Pantazis, D., & Oliva, A. (2014). Resolving human object
770 recognition in space and time. *Nature Neuroscience*, *17*(3), 455–462.
771 https://doi.org/10.1038/nn.3635
772 Cichy, Radoslaw Martin, Pantazis, D., & Oliva, A. (2016). Similarity-Based Fusion of MEG
773 and fMRI Reveals Spatio-Temporal Dynamics in Human Cortex During Visual Object
774 Recognition. *Cerebral Cortex*, *26*(8), 3563–3579.
775 https://doi.org/10.1093/cercor/bhw135
776 Desimone, R., & Duncan, J. (1995). Neural Mechanisms of Selective Visual Attention.
777 *Annual Review of Neuroscience*, *18*(1), 193–222.
778 https://doi.org/10.1146/annurev.ne.18.030195.001205
779 Dienes, Z. (2011). Bayesian Versus Orthodox Statistics: Which Side Are You On?
780 *Perspectives on Psychological Science*, *6*(3), 274–290.
781 https://doi.org/10.1177/1745691611406920
782 Dosenbach, N. U. F., Visscher, K. M., Palmer, E. D., Miezin, F. M., Wenger, K. K., Kang, H.
783 C., Burgund, E. D., Grimes, A. L., Schlaggar, B. L., & Petersen, S. E. (2006). A Core
784 System for the Implementation of Task Sets. *Neuron*, *50*(5), 799–812.
785 https://doi.org/10.1016/j.neuron.2006.04.031
786 Duncan, J. (2001). An adaptive coding model of neural function in prefrontal cortex. *Nature*
787 *Reviews Neuroscience*, *2*(11), 820–829. https://doi.org/10.1038/35097575
788 Duncan, J. (2010). The multiple-demand (MD) system of the primate brain: mental programs
789 for intelligent behaviour. *Trends in Cognitive Sciences*, *14*(4), 172–179.
790 https://doi.org/10.1016/j.tics.2010.01.004
791 Duncan, J., Assem, M., & Shashidhara, S. (2020). Integrated Intelligence from Distributed
792 Brain Activity. *Trends in Cognitive Sciences*, *24*(10), 838–852.
793 https://doi.org/10.1016/j.tics.2020.06.012

bioRxiv preprint doi: https://doi.org/10.1101/2021.02.28.433294; this version posted March 1, 2021. The copyright holder for this preprint (which was not certified by peer review) is the author/funder. All rights reserved. No reuse allowed without permission.

794 Duncan, J., & Owen, A. M. (2000). Common regions of the human frontal lobe recruited by
795 diverse cognitive demands. *Trends in Neurosciences*, *23*(10), 475–483.
796 https://doi.org/10.1016/S0166-2236(00)01633-7
797 Fedorenko, E., Duncan, J., & Kanwisher, N. (2013). Broad domain generality in focal regions
798 of frontal and parietal cortex. *Proceedings of the National Academy of Sciences*,
799 *110*(41), 16616–16621. https://doi.org/10.1073/pnas.1315235110
800 Fox, M. D., Snyder, A. Z., Vincent, J. L., Corbetta, M., Essen, D. C. V., & Raichle, M. E.
801 (2005). The human brain is intrinsically organized into dynamic, anticorrelated
802 functional networks. *Proceedings of the National Academy of Sciences*, *102*(27),
803 9673–9678. https://doi.org/10.1073/pnas.0504136102
804 Fusi, S., Miller, E. K., & Rigotti, M. (2016). Why neurons mix: high dimensionality for higher
805 cognition. *Current Opinion in Neurobiology*, *37*, 66–74.
806 https://doi.org/10.1016/j.conb.2016.01.010
807 Goddard, E., Carlson, T. A., & Woolgar, A. (2019). Spatial and feature-selective attention
808 have distinct effects on population-level tuning. *BioRxiv*, 530352.
809 https://doi.org/10.1101/530352
810 Gold, J. I., & Shadlen, M. N. (2007). The Neural Basis of Decision Making. *Annual Review of*
811 *Neuroscience*, *30*(1), 535–574.
812 https://doi.org/10.1146/annurev.neuro.29.051605.113038
813 Grootswagers, T., Wardle, S. G., & Carlson, T. A. (2016). Decoding Dynamic Brain Patterns
814 from Evoked Responses: A Tutorial on Multivariate Pattern Analysis Applied to Time
815 Series Neuroimaging Data. *Journal of Cognitive Neuroscience*, *29*(4), 677–697.
816 https://doi.org/10.1162/jocn_a_01068
817 Harel, A., Kravitz, D. J., & Baker, C. I. (2014). Task context impacts visual object processing
818 differentially across the cortex. *Proceedings of the National Academy of Sciences*,
819 *111*(10), E962–E971. https://doi.org/10.1073/pnas.1312567111

bioRxiv preprint doi: https://doi.org/10.1101/2021.02.28.433294; this version posted March 1, 2021. The copyright holder for this preprint (which was not certified by peer review) is the author/funder. All rights reserved. No reuse allowed without permission.

820 Haynes, J.-D. (2015). A Primer on Pattern-Based Approaches to fMRI: Principles, Pitfalls,
821 and Perspectives. *Neuron*, *87*(2), 257–270.
822 https://doi.org/10.1016/j.neuron.2015.05.025
823 Hebart, M. N., & Baker, C. I. (2017). Deconstructing multivariate decoding for the study of
824 brain function. *NeuroImage*. https://doi.org/10.1016/j.neuroimage.2017.08.005
825 Hebart, M. N., Bankson, B. B., Harel, A., Baker, C. I., & Cichy, R. M. (2018). The
826 representational dynamics of task and object processing in humans. *Elife*, *7*, e32816.
827 Heekeren, H. R., Marrett, S., & Ungerleider, L. G. (2008). The neural systems that mediate
828 human perceptual decision making. *Nature Reviews Neuroscience*, *9*(6), 467–479.
829 https://doi.org/10.1038/nrn2374
830 Hon, N., Epstein, R. A., Owen, A. M., & Duncan, J. (2006). Frontoparietal Activity with
831 Minimal Decision and Control. *Journal of Neuroscience*, *26*(38), 9805–9809.
832 https://doi.org/10.1523/JNEUROSCI.3165-06.2006
833 Jackson, J. B., Feredoes, E., Rich, A. N., Lindner, M., & Woolgar, A. (2020). Concurrent
834 neuroimaging and neurostimulation reveals a causal role for dlPFC in coding of task-
835 relevant information. *BioRxiv*, 2020.04.22.054742.
836 https://doi.org/10.1101/2020.04.22.054742
837 Jackson, J., Rich, A. N., Williams, M. A., & Woolgar, A. (2016). Feature-selective Attention in
838 Frontoparietal Cortex: Multivoxel Codes Adjust to Prioritize Task-relevant
839 Information. *Journal of Cognitive Neuroscience*, *29*(2), 310–321.
840 https://doi.org/10.1162/jocn_a_01039
841 Jackson, J., & Woolgar, A. (2018). Adaptive coding in the human brain: Distinct object
842 features are encoded by overlapping voxels in frontoparietal cortex. *Cortex*.
843 https://doi.org/10.1016/j.cortex.2018.07.006
844 Jeffreys, H. (1998). *The Theory of Probability*. OUP Oxford.

bioRxiv preprint doi: https://doi.org/10.1101/2021.02.28.433294; this version posted March 1, 2021. The copyright holder for this preprint (which was not certified by peer review) is the author/funder. All rights reserved. No reuse allowed without permission.

Jehee, J. F. M., Ling, S., Swisher, J. D., Bergen, R. S. van, & Tong, F. (2012). Perceptual Learning Selectively Refines Orientation Representations in Early Visual Cortex. *Journal of Neuroscience*, *32*(47), 16747–16753. https://doi.org/10.1523/JNEUROSCI.6112-11.2012

Kadohisa, M., Petrov, P., Stokes, M., Sigala, N., Buckley, M., Gaffan, D., Kusunoki, M., & Duncan, J. (2013). Dynamic Construction of a Coherent Attentional State in a Prefrontal Cell Population. *Neuron*, *80*(1), 235–246. https://doi.org/10.1016/j.neuron.2013.07.041

Kass, R. E., & Raftery, A. E. (1995). Bayes Factors. *Journal of the American Statistical Association*, *90*(430), 773–795. https://doi.org/10.1080/01621459.1995.10476572

Kleiner, M., Brainard, D., & Pelli, D. (2007). What's new in Psychtoolbox-3? *Perception 36 ECVP Abstract Supplement*.

Kriegeskorte, N., Goebel, R., & Bandettini, P. (2006). Information-based functional brain mapping. *Proceedings of the National Academy of Sciences*, *103*(10), 3863–3868. https://doi.org/10.1073/pnas.0600244103

Kriegeskorte, N., Mur, M., & Bandettini, P. A. (2008). Representational similarity analysis - connecting the branches of systems neuroscience. *Frontiers in Systems Neuroscience*, *2*. https://doi.org/10.3389/neuro.06.004.2008

Li, S., Ostwald, D., Giese, M., & Kourtzi, Z. (2007). Flexible Coding for Categorical Decisions in the Human Brain. *Journal of Neuroscience*, *27*(45), 12321–12330. https://doi.org/10.1523/JNEUROSCI.3795-07.2007

Löffler, A., Haggard, P., & Bode, S. (2019). Decoding Changes of Mind in Voluntary Action—Dynamics of Intentional Choice Representations. *Cerebral Cortex*. https://doi.org/10.1093/cercor/bhz160

bioRxiv preprint doi: https://doi.org/10.1101/2021.02.28.433294; this version posted March 1, 2021. The copyright holder for this preprint (which was not certified by peer review) is the author/funder. All rights reserved. No reuse allowed without permission.

869 Morey, R. D., & Rouder, J. N. (2011). Bayes factor approaches for testing interval null
870 hypotheses. *Psychological Methods*, *16*(4), 406–419.
871 https://doi.org/10.1037/a0024377
872 Morey, R. D., & Rouder, J. N. (2018). *BayesFactor: Computation of Bayes Factors for*
873 *Common Designs*. https://CRAN.R-project.org/package=BayesFactor
874 Oostenveld, R., Fries, P., Maris, E., & Schoffelen, J.-M. (2011). FieldTrip: Open Source
875 Software for Advanced Analysis of MEG, EEG, and Invasive Electrophysiological
876 Data. *Computational Intelligence and Neuroscience*, *2011*, 1–9.
877 https://doi.org/10.1155/2011/156869
878 Oosterhof, N. N., Connolly, A. C., & Haxby, J. V. (2016). CoSMoMVPA: Multi-Modal
879 Multivariate Pattern Analysis of Neuroimaging Data in Matlab/GNU Octave. *Frontiers*
880 *in Neuroinformatics*, *10*. https://doi.org/10.3389/fninf.2016.00027
881 Pelli, D. G. (1997). The VideoToolbox software for visual psychophysics: Transforming
882 numbers into movies. *Spatial Vision*, *10*(4), 437–442.
883 Pestilli, F., & Carrasco, M. (2005). Attention enhances contrast sensitivity at cued and
884 impairs it at uncued locations. *Vision Research*, *45*(14), 1867–1875.
885 https://doi.org/10.1016/j.visres.2005.01.019
886 Posner, M. I. (1980). Orienting of attention. *Quarterly Journal of Experimental Psychology*,
887 *32*(1), 3–25. https://doi.org/10.1080/00335558008248231
888 Pratte, M. S., Ling, S., Swisher, J. D., & Tong, F. (2013). How attention extracts objects from
889 noise. *Journal of Neurophysiology*, *110*(6), 1346–1356.
890 https://doi.org/10.1152/jn.00127.2013
891 Rao, S. C., Rainer, G., & Miller, E. K. (1997). Integration of What and Where in the Primate
892 Prefrontal Cortex. *Science*, *276*(5313), 821–824.
893 https://doi.org/10.1126/science.276.5313.821

bioRxiv preprint doi: https://doi.org/10.1101/2021.02.28.433294; this version posted March 1, 2021. The copyright holder for this preprint (which was not certified by peer review) is the author/funder. All rights reserved. No reuse allowed without permission.

894 Ratcliff, R., & McKoon, G. (2007). The Diffusion Decision Model: Theory and Data for Two-
895 Choice Decision Tasks. *Neural Computation*, *20*(4), 873–922.
896 https://doi.org/10.1162/neco.2008.12-06-420
897 Rens, N., Bode, S., Burianová, H., & Cunnington, R. (2017). Proactive Recruitment of
898 Frontoparietal and Salience Networks for Voluntary Decisions. *Frontiers in Human*
899 *Neuroscience*, *11*. https://doi.org/10.3389/fnhum.2017.00610
900 Rigotti, M., Barak, O., Warden, M. R., Wang, X.-J., Daw, N. D., Miller, E. K., & Fusi, S.
901 (2013). The importance of mixed selectivity in complex cognitive tasks. *Nature*,
902 *497*(7451), 585–590. https://doi.org/10.1038/nature12160
903 Rorden, C., & Brett, M. (2000). *Stereotaxic Display of Brain Lesions* [Research article].
904 Behavioural Neurology. https://doi.org/10.1155/2000/421719
905 Rouder, J. N., Morey, R. D., Speckman, P. L., & Province, J. M. (2012). Default Bayes
906 factors for ANOVA designs. *Journal of Mathematical Psychology*, *56*(5), 356–374.
907 https://doi.org/10.1016/j.jmp.2012.08.001
908 Rouder, J. N., Speckman, P. L., Sun, D., Morey, R. D., & Iverson, G. (2009). Bayesian t
909 tests for accepting and rejecting the null hypothesis. *Psychonomic Bulletin & Review*,
910 *16*(2), 225–237. https://doi.org/10.3758/PBR.16.2.225
911 Sàenz, M., Buraĉas, G. T., & Boynton, G. M. (2003). Global feature-based attention for
912 motion and color. *Vision Research*, *43*(6), 629–637. https://doi.org/10.1016/S0042-
913 6989(02)00595-3
914 Seeley, W. W., Menon, V., Schatzberg, A. F., Keller, J., Glover, G. H., Kenna, H., Reiss, A.
915 L., & Greicius, M. D. (2007). Dissociable Intrinsic Connectivity Networks for Salience
916 Processing and Executive Control. *Journal of Neuroscience*, *27*(9), 2349–2356.
917 https://doi.org/10.1523/JNEUROSCI.5587-06.2007
918 Sigala, N., Kusunoki, M., Nimmo-Smith, I., Gaffan, D., & Duncan, J. (2008). Hierarchical
919 coding for sequential task events in the monkey prefrontal cortex. *Proceedings of the*

bioRxiv preprint doi: https://doi.org/10.1101/2021.02.28.433294; this version posted March 1, 2021. The copyright holder for this preprint (which was not certified by peer review) is the author/funder. All rights reserved. No reuse allowed without permission.

National Academy of Sciences, *105*(33), 11969–11974. https://doi.org/10.1073/pnas.0802569105

Stiers, P., Mennes, M., & Sunaert, S. (2010). Distributed task coding throughout the multiple demand network of the human frontal–insular cortex. *NeuroImage*, *52*(1), 252–262. https://doi.org/10.1016/j.neuroimage.2010.03.078

Stokes, M. G., Kusunoki, M., Sigala, N., Nili, H., Gaffan, D., & Duncan, J. (2013). Dynamic Coding for Cognitive Control in Prefrontal Cortex. *Neuron*, *78*(2), 364–375. https://doi.org/10.1016/j.neuron.2013.01.039

Vincent, J. L., Kahn, I., Snyder, A. Z., Raichle, M. E., & Buckner, R. L. (2008). Evidence for a Frontoparietal Control System Revealed by Intrinsic Functional Connectivity. *Journal of Neurophysiology*, *100*(6), 3328–3342. https://doi.org/10.1152/jn.90355.2008

Wagenmakers, E.-J. (2007). A practical solution to the pervasive problems ofp values. *Psychonomic Bulletin & Review*, *14*(5), 779–804. https://doi.org/10.3758/BF03194105

Waskom, M. L., Kumaran, D., Gordon, A. M., Rissman, J., & Wagner, A. D. (2014). Frontoparietal Representations of Task Context Support the Flexible Control of Goal-Directed Cognition. *Journal of Neuroscience*, *34*(32), 10743–10755. https://doi.org/10.1523/JNEUROSCI.5282-13.2014

Wetzels, R., Matzke, D., Lee, M. D., Rouder, J. N., Iverson, G. J., & Wagenmakers, E.-J. (2011). Statistical Evidence in Experimental Psychology: An Empirical Comparison Using 855 t Tests. *Perspectives on Psychological Science*, *6*(3), 291–298. https://doi.org/10.1177/1745691611406923

White, A. L., & Carrasco, M. (2011). Feature-based attention involuntarily and simultaneously improves visual performance across locations. *Journal of Vision*, *11*(6), 15–15. https://doi.org/10.1167/11.6.15

bioRxiv preprint doi: https://doi.org/10.1101/2021.02.28.433294; this version posted March 1, 2021. The copyright holder for this preprint (which was not certified by peer review) is the author/funder. All rights reserved. No reuse allowed without permission.

945 Woolgar, A., Afshar, S., Williams, M. A., & Rich, A. N. (2015). Flexible Coding of Task Rules
946 in Frontoparietal Cortex: An Adaptive System for Flexible Cognitive Control. *Journal*
947 *of Cognitive Neuroscience*, *27*(10), 1895–1911.
948 https://doi.org/10.1162/jocn_a_00827
949 Woolgar, A., Golland, P., & Bode, S. (2014). Coping with confounds in multivoxel pattern
950 analysis: What should we do about reaction time differences? A comment on Todd,
951 Nystrom & Cohen 2013. *NeuroImage*, *98*, 506–512.
952 https://doi.org/10.1016/j.neuroimage.2014.04.059
953 Woolgar, A., Hampshire, A., Thompson, R., & Duncan, J. (2011). Adaptive Coding of Task-
954 Relevant Information in Human Frontoparietal Cortex. *Journal of Neuroscience*,
955 *31*(41), 14592–14599. https://doi.org/10.1523/JNEUROSCI.2616-11.2011
956 Woolgar, A., Jackson, J., & Duncan, J. (2016). Coding of Visual, Auditory, Rule, and
957 Response Information in the Brain: 10 Years of Multivoxel Pattern Analysis. *Journal*
958 *of Cognitive Neuroscience*, *28*(10), 1433–1454.
959 https://doi.org/10.1162/jocn_a_00981
960 Woolgar, A., Thompson, R., Bor, D., & Duncan, J. (2011). Multi-voxel coding of stimuli, rules,
961 and responses in human frontoparietal cortex. *NeuroImage*, *56*(2), 744–752.
962 https://doi.org/10.1016/j.neuroimage.2010.04.035
963 Woolgar, A., Williams, M. A., & Rich, A. N. (2015). Attention enhances multi-voxel
964 representation of novel objects in frontal, parietal and visual cortices. *NeuroImage*,
965 *109*, 429–437. https://doi.org/10.1016/j.neuroimage.2014.12.083
966